RSC Advances

ROYAL SOCIETY OF CHEMISTRY

www.rsc.org/advances

Cite this: DOI: 10.1039/c0xx00000x

www.rsc.org/xxxxxx

PAPER

Bimodal "matrix-free" polymer nanocomposites

Ying Li,*[a] Lei Wang,[b] Bharath Natarajan,[a] Peng Tao,[a,c] Brian C. Benicewicz,[b] Chaitanya Ullal[a] and Linda S. Schadler[a]

Received (in XXX, XXX) Xth XXXXXXXXX 20XX, Accepted Xth XXXXXXXXX 20XX

DOI: 10.1039/b000000x

Maximum performance enhancement in polymer nanocomposites is predicated on the simultaneous realization of maximum filler loading, controlled filler dispersion and structural integrity. Through the example of high refractive index ZrO_2/polydimethylsiloxane encapsulants for LEDs for enhanced light extraction efficiency, this paper demonstrates that all three properties can be achieved by eliminating the matrix in a single component polymer nanocomposite. Surface bound polymer brushes serve as both the matrix, and stabilizing agent to ensure uniform filler dispersion. The use of multimodal brush configurations that are at least bimodal is the key enabler. This provides sufficient crowding near the particle surface to screen core-core attraction, as well as entanglement between sparsely grafted long brushes to prevent premature cracking. A further widening of the applicability and processing windows are achieved by introducing crosslinkable moieties into the brushes.

Introduction

Conventional polymer nanocomposites consist of 1) inorganic nanofiller as a property/performance booster, 2) a polymeric matrix providing processability and holding the reinforcements together into a solid, and 3) surface ligands to control nanofiller dispersion, essential to delivering the promised performance enhancement (Scheme 1).[1-3] To obtain greater property reinforcement, a large volume fraction of nanofiller (v_{filler}) is often desired, especially for optical nanocomposites.[4, 5] However, the probability for macro-phase separation tends to be larger at higher volume fraction. To maximize nanoparticle loading while maintaining uniform particle dispersion, v_{matrix} should be zero. In this case, surface grafted polymer brushes act as both matrix material, and stabilizing agent. Without the presence of the matrix phase, macro-phase separation is effectively prevented since there is only one component in the "matrix-free" nanocomposite system, provided that the ligands are chemically bound to the nanoparticle surface.

An analogous matrix-free system is the so-called organic/inorganic "solvent-free nanofluid", whose fluidity is suited for applications in heat-transfer fluids, lubricants, and liquid electrolytes.[6-10] Solid-state polymer nanocomposites, on the other hand, require a higher level of structural integrity. Tchoul *et al.* first demonstrated a mechnically robust matrix-free assembly of inorganic nanoparticles surface grafted with thermoplastic polymer brushes.[11] Polymer brush chain interpenetration and entanglement, which occurs only above a critical molecular weight for entanglement,[12] serves as physical cross-links to ensure good mechanical properties.[13]

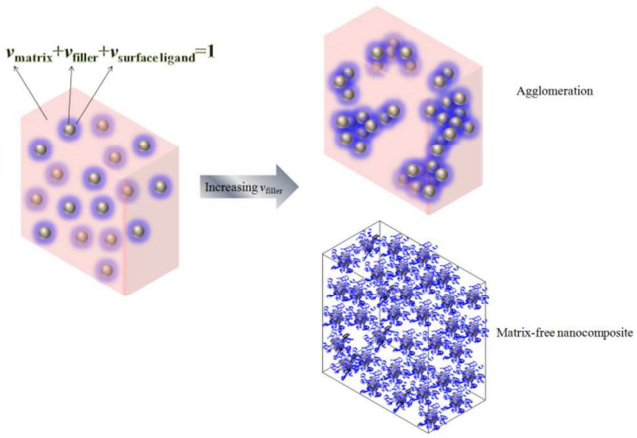

Scheme 1 (Left) Illustration of a conventional three-component polymer nanocomposite system and (right) comparison of nanoparticle agglomeration versus matrix-free nanocomposite for maximized nanocomposite performance enhancement.

Alternatively, in the absence of entanglements, mechanical integrity can be provided by chemical cross-linking, which is especially important for thermoset polymer nanocomposites with a T_g below room temperature. A low T_g brush can be useful for promoting flow and moldability, while setting the meso- or macroscopic assemblies of grafted nanoparticles into desired architectures can be enabled by cross-linkable brush polymers. Using two kinds of complementary reactive polymer brush grafted SiO_2 nanoparticles, Dach *et al.* synthesized chemically cross-linked "matrix-free" nanocomposites.[14] However, the reported shear moduli of the cross-linked nanocomposites were low, due to incomplete network formation between the two immiscible polymer brushes. A suggested solution is to use the same crosslinkable moiety for all the SiO_2 particles. The van der Waals (vdW) core-core attraction between high refractive index metal oxide (e.g. TiO_2 or ZrO_2) nanoparticles within a polydimethylsiloxane (PDMS) matrix is often much higher than the thermal fluctuations at room temperature (5 to 10 k_BT), which encourages particle core – core agglomeration.[15-18] Intuition suggests that a densely grafted long chain polymer brush would

screen this core-core attraction and also enable entanglement. However, achieving both high graft density and high molecular weight of a polymer brush is not only experimentally challenging but reduces the achievable v_{filler}.

Bidispersity or polydispersity of surface grafted polymer brushes has been used recently to promote metal oxide nanoparticle dispersion in high molecular weight polymers.[19-22] A high graft density short brush encourages enthalpic screening and the long low graft density brushes encourage entropy-driven mixing of the matrix long brush chains.[15, 17, 23, 24] For "matrix-free" polymer nanocomposites where filler dispersal is no longer relevant, the polydispersity of the grafted brush is still useful, providing core repulsion and brush entanglement at low brush volume. Since monomer crowding near the particle surface determines the shielding of core-core attraction,[25] it is reasonable and necessary to decrease crowding of long brush chains farther from the particle surface to allow entanglement while reducing the total brush volume fraction, $v_{\text{surface ligand}}$.

Results and discussion

In the following dissusion, we will use high refractive index ZrO_2 filled PDMS nanocomposites as a model system to demonstrate the basic principles as well as practical applications of "matrix-free" nanocomposites.

Refractive index engineering

Spherical ZrO_2 nanoparticles were synthesized using a non-aqueous surfactant-free synthetic approach adapted from the procedure reported by Garnweitner *et al*.[26] Commercially available carboxyalkyl-terminated PDMS brushes and phosphate-terminated brushes obtained through phosphoryl chloride modification were used to graft onto the nanoparticle.[15] There are three decisive advantages of the synthesized ZrO_2 nanoparticles for use as optical nanofillers. First, the near monodisperse, ~1.9 nm in radius nanoscale ZrO_2 particles reduce light loss from scattering when homogenously dispersed in a transparent polymer (see Figure S1 (a) for TEM and size distribution). Second, the cubic ZrO_2 (see Figure S1 (b) for XRD pattern), with an isotropic refractive index of 2.2 at 589 nm,[27] is a desirable refractive index enhancer with no significant light scattering loss resulting from grain boundaries.[28] Third, since there is no additional surfactant (other than the solvent benzyl alcohol) intentionally introduced in the nanoparticle synthesis, the surfaces of the as-synthesized nanoparticles are highly accessible for post-functionalization. Monomodal, bimodal, and trimodal PDMS grafted nanoparticles, ZrO_2_1k, ZrO_2_1k_10k, and ZrO_2_1k_36k_10k, respectively, named according to the molecular weight of the brushes, were prepared via a multiple-step "grafting-to" process, as shown in Scheme 2. Note that the sequence of the "grafting-to" reaction plays an important role in obtaining grafted nanoparticles with proper graft densities. The purpose of grafting the shortest carboxyalkyl-terminated PDMS brush (1k) before the other "grafting-to" reactions is twofold: 1) One inherent limitation of the "grafting-to" method is the rapidly decreased graft density with increased brush length attributable to the increased difficulties for longer brush diffusing through the grafting surface.[11, 15] The relatively densely grafted 1k PDMS brush provides initial stable solvent suspension for the following "grafting-to" reaction. 2) Compared to the phosphate-terminated PDMS brushes, the anchoring of the carboxyalkyl-terminated PDMS brush is relatively weak,[29, 30] leaving adequate probabilities for sequential grafting of phosphate-terminated PDMS brushes to prepare bimodal or even multimodal polymer brush grafted nanoparticles. For the phosphate-terminated PDMS brushes (36k and 10k), on the other hand, it is important to graft the longer brush first and then back fill the remaining grafting sites with shorter brush to ensure that the existence of the grafted brush does not impose a significant barrier for the shorter brush to reach the grafting surface.

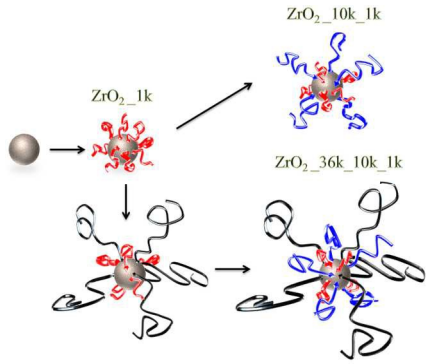

Scheme 2 Schematic illustration of the preparation of ZrO_2_1k, ZrO_2_1k_10k, and ZrO_2_1k_36k_10k nanoparticles via a multiple-step "grafting-to" process.

The v_{filler} of ZrO_2_1k, ZrO_2_1k_10k, and ZrO_2_1k_36k_10k nanoparticles were estimated as 79 wt%, 53 wt%, and 44 wt%, respectively, using thermo gravimetric analysis (TGA) weight loss measurement (Figure S2). To get a better understanding of grafted nanoparticle dimensions and architecture, each step of the "grafting-to" reaction was also monitored. The graft density of each PDMS brush was calculated first based on the corresponding weight loss ratio and the number of grafting chains (determined by TGA after each step of "grafting-to"), and surface area of nanoparticles using:[31]

$$\sigma = (wN_A/M_n)/(4\pi a^2 n)$$

where w, N_A, and n are the weight of polymers, Avogadro's number, and the number of nanoparticles, respectively. As listed in Table 1 (see Supplementary Information for a detailed description of the calculation), at low enough graft density, $\sigma < 1/R_g{}^2$, we assume that individual chains take mushroom-like conformations on the grafting surface with a thickness of the radius of gyration.[32, 33]

Table 1 Dimensions and graft densities of PDMS brushes.[a]

Brush	r/R_g	$1/R_g{}^2$	σ (ch/nm^2)		
			ZrO_2_1k	ZrO_2_1k_10k	ZrO_2_1k_36k_10k
1k	1.9	0.96	0.28	0.20	0.12
10k	0.59	0.10	-	0.10	0.05
36k	0.31	0.03	-	-	0.02

[a] Nanoparticle core radius, brush radius of gyration and graft density are denoted by r, R_g, and σ, respectively.

Cite this: DOI: 10.1039/c0xx00000x

www.rsc.org/xxxxxx

PAPER

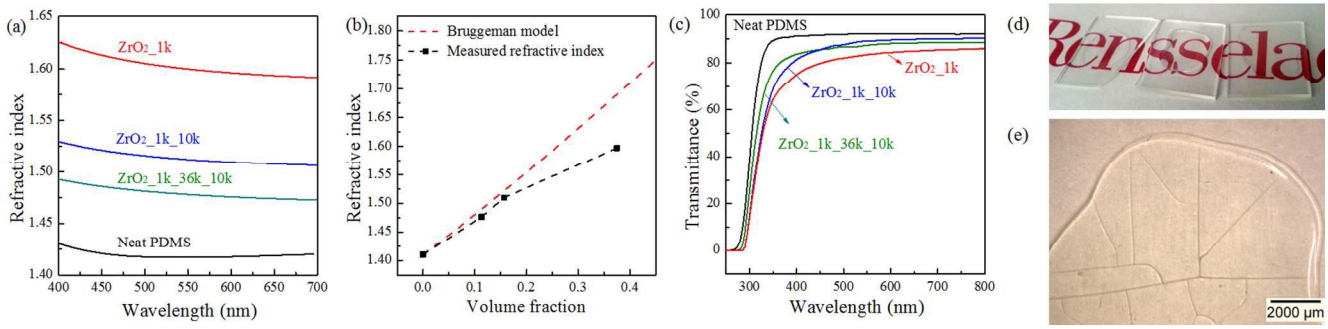

Fig. 1 (a) Refractive index dispersion of neat PDMS and "matrix-free" ZrO_2/PDMS nanocomposites with three different v_{filler}. (b) Comparison of measured refractive indices at 633 nm with the Bruggeman model. (c) UV-Vis spectra of the three types of "matrix-free" nanocomposites. (d) Photograph shows the appearance of the ~0.5 mm thick samples. (e) Photograph showing crack propagation in the ZrO_2_1k sample after one month.

After solvent removal, the visual appearance of the grafted nanoparticle films remains highly transparent, indicating uniform dispersion and distribution of nanoparticle cores within the PDMS brush polymer. Therefore, the terms "grafted nanoparticles" and "matrix-free nanocomposite" are used interchangeably.

With increasing v_{filler}, the measured refractive index increased up to 14 % (ZrO_2_1k) compared to neat PDMS, as shown in Fig. 1 (a). The dependence of the effective refractive index of the "matrix-free" nanocomposite on its v_{filler} was described by the Bruggeman formula in Fig. 1 (b),[34]

$$v_{filler}\,[(\varepsilon_p - \varepsilon_{eff})/(\varepsilon_p + 2\varepsilon_{eff})] + (1 - v_{filler})[(\varepsilon_m - \varepsilon_{eff})/(\varepsilon_m + 2\varepsilon_{eff})] = 0$$

where ε_p and $\varepsilon_m$are the dielectric constants of the nanoparticles and matrix, respectively, and ε_{eff} the effective dielectric constant of the nanocomposite. For the ZrO_2_1k sample with the highest v_{filler}, there is a significant deviation from theoretical prediction. The discrepancy could be due to decreased refractive index of the nanoparticles compared to the bulk material as a result of quantum size effects.[35] Another possible explanation is the complex interaction between adjacent nanoparticles when the interparticle distance is smaller than the particle size (r/R_g~ 1.9). For example, interfering wave functions of electrons may change the dipole polarizability.[36] As shown in Fig. 1 (c), all the nanocomposites show high transparency, comparable to neat PDMS in the visible light range (the ~9% intensity loss for the neat PDMS sample in the 400 to 800 nm range is due to reflection losses at the air/film/glass slide interfaces[37]). Since both the ZrO_2 nanoparticles and PDMS are assumed to be intrinsically transparent to visible light, Rayleigh scattering becomes the dominant transparency loss mechanism.[5, 38, 39] The effective suppression of Rayleigh scattering in the nanocomposites is direct evidence of sufficiently uniform dispersion of the ZrO_2. The slight decrease in the transmittance (~5%) of the ZrO_2_1k sample can be attributed to the less robust stabilizing effect of the 1k carboxyalkyl-terminated PDMS brushes compared to the 10k and 36k phosphate-terminated ones.

The "matrix-free" nanocomposite approach is applicable across many other metal oxide / polymer hybrid systems. Two requirements must be met in order for the transparent "matrix-free" approach to be implemented successfully. First, the nanoparticle must be sufficiently small (typically less than 5 nm in diameter) such that the translational entropy favoring randomized particle distribution becomes more dominant and the particle core-core attraction can be suppressed more easily. Second, due to the inefficient packing of nanoparticles, at least one population of the polymer brushes, the 1k brush in this case, must be smaller than the particle and be able to isotropically fill the interstitial space between the nanoparticle cores to avoid particle percolation. TiO_2_36k_10k nanoparticles studied previously,[15] with higher effective vdW core-core attraction (graft densities of 10k and 36k brushes are 0.03 and 0.01 ch/nm^2, respectively) and bigger particle size (r/R_g ~0.77 for the 10k brush), appeared to be cloudy after complete solvent removal (Figure S3). To study grafted nanoparticle packing more systematically, useful tools include genetic algorithm and Monte Carlo simulations,[40] assuming that the brush is in a mushroom conformation on the grafting surface. For concentrated and semi-dilute polymer brush regimes, experimental and theoretical studies on assembling and ordering of solvent-free hairy nanoparticles has also been conducted to relate the architecture of the nanoparticle assembles and their physical characteristics.[41-43]

Applications in LED encapsulation

Incorporating uniformly dispersed high refractive index metal oxide nanoparticles into encapsulant polymers is a promising strategy to reduce the refractive index mismatch between the LED die and its surrounding medium, and therefore enhance the light extraction efficiency.[5, 44] The ZrO_2_1k sample with the highest refractive index enhancement and optical transparency seems to be the most promising candidate for practical optical applications. However, after aging in an ambient environment for a few weeks, the ZrO_2_1k sample cracked, as shown in Fig. 1 (e). The cracks, probably caused by capillary forces arising from solvent evaporation, are not observed in the ZrO_2_1k_10k and

ZrO_2_1k_36k_10k samples. The poor crack resistance of the ZrO_2_1k sample can be attributed to the lack of entanglement for the 1 kg mol^{-1} short brush chains. Two parameters need to be investigated in order to understand this phenomenon: the entanglement molecular weight, M_e, denoting the average molecular weight spacing between entanglement junctions, and the critical molecular weight, M_c, which separates the dependence of zero-shear viscosity on molecular weight for short and long chains.[45] The published values of M_e for linear PDMS are around 12,000 g mol^{-1} and M_c ranges from 21,000 to 29,000 g mol^{-1}, which agree well with the empirical relation M_c / M_e ~2 for amorphous melts.[12, 46-49] The molecular weight of the longest brush in the ZrO_2_1k_10k sample is only half of M_c, thus cracking could also be expected in this sample. However, the average number of chain ends per polymer can affect the value of M_c.[45, 50] Utilizing an immiscible polymer blend whose interface is reinforced with corresponding diblock copolymers, Kramer and co-workers have suggested that, while the onset of entangled behavior in a polymer melt requires an average of two entanglements per chain (consistent with M_c ~2 M_e), one "entanglement" between each block and its corresponding homopolymer is enough to have stress transfer at the interface.[50, 51] This is consistent with the observation of Choi et al. that pronounced interactions between entanglements of surface-grafted polymer chains give rise to significant increased resistance to fracture of the 'quasi-one-component' nanocomposite.[13] Since one end of the 10k brush has been chemically grafted onto the nanoparticle surface, it is also reasonable to postulate that having one "entanglement" for each 10k brush chain (requires a molecular weight half of M_c) is sufficient to hinder cracking.

ZrO_2_1k_10k samples were used for LED encapsulation. Using a well-controlled encapsulation process, commercial pure silicone and nanocomposite encapsulant (a silicone shell was molded to protect the un-crosslinked nanocomposite) with identical hemi-spherical geometry were mounted onto LEDs for optical output characterization, as shown in Fig. 2. Commercial silicone encapsulated red and green LEDs exhibit an average of 38% and 16% optical output power enhancement, respectively, compared to un-encapsulated LEDs, while the nanocomposite encapsulated LEDs exhibit an average of 48% and 24% enhancement. Ma *et al.* modeled and experimentally investigated the influence of the refractive index of the LED encapsulant on light-extraction efficiency due to high refractive index encapsulants, using low-power LEDs.[52] In our case, the light-extraction enhancement is less significant than the theoretical prediction in Ma's work because surface-roughened high-power LEDs were used in the current study. Less significant light extraction improvement was observed in blue LEDs. Careful examination of the appearance of the "matrix-free" ZrO_2/PDMS nanocomposite after solvent removal reveals a slightly yellowed color. It has been reported previously that the ZrO_2 nanoparticles synthesized using a non-aqueous approach resulted in a slightly yellow solvent suspension before surface modification.[26] The yellow-colored organic species leads to absorption of blue light and therefore reduced light extraction enhancement (see Figure S4 for rationale).

To further validate the performance of the matrix-free nanocomposite as novel LED encapsulant, an accelerated aging test was conducted.The reliability of the encapsulant material is directly related to the durability of a LED package. In a preliminary reliability evaluation, the aging tests were performed in a chamber placed in a constant temperature (24±2°C) and humidity (60±5%) environment, and the chamber is equipped with a programmable D.C. power supply, an air-cooling system, and multi-channel temperature/current monitoring systems. The optical output powers of unencapsulated, silicone- and nanoparticle-encapsulated green LEDs were measured as a function of time. Two sets of experiments were conducted. For the first set of experiments, the LEDs were held at 100±3% mA for 500 hours and then 350±3% mA for 500 hours. The other set of experiments started at 500 mA for 500 hours and then 1000±3% mA for 500 hours to perform a high intensity test and accelerate aging. The optical output was normalized to the onset state for each set of experiments accordingly. As shown in Fig. 3, the nanocomposite-encapsulated LEDs exhibit high reliability (more than 90% lumen maintenance) at up to 1 A driving current. Since commercial high-refractive-index silicone encapsulant often suffers from poor processability and thermal stability due to the high phenyl content,[15, 16] the matrix-free nanocomposite presents a promising alternative for highly efficient LED devices and new luminaire design. It is expected that with an improved nanoparticle synthetic method the light extraction efficiency and reliability of encapsulated LEDs can be further improved.

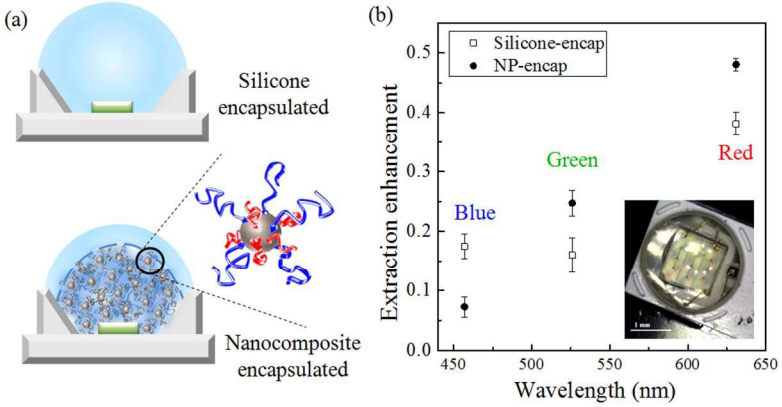

Fig.2 (a) Illustrative cross-section of commercial silicone encapsulated LED and nanocomposite encapsulated LED. (b) Light extraction enhancement after encapsulation of commercial silicone and the ZrO_2_1k_10k nanocomposite/silicone double-layer. Inset photograph of a nanocomposite encapsulated green LED.

Cite this: DOI: 10.1039/c0xx00000x

www.rsc.org/xxxxxx

PAPER

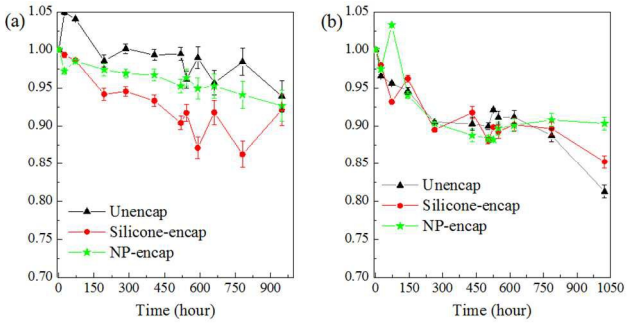

Fig. 3 The degradation of optical output power for different green LED packages. LED forward current was maintained at (a) 100±3% mA for 500 hours and then 350±3% mA for 500 hours; (b) 500±3% mA for 500 hours and then 1000±3% mA for 500 hours.

Cross-linkable "matrix-free" nanocomposites

The transparent high refractive index "matrix-free" ZrO_2/PDMS nanocomposites discussed thus far can be reversibly dissolved in chloroform. For improved structural integrity, the incorporation of a cross-linkable group into the brush polymer was examined. As a proof-of-concept, PDMS brushes with a phosphonic acid group on one end serving as a robust anchor onto the nanoparticle surface, and a cross-linkable vinyl group on the other end were synthesized through a hydrosilylation reaction between α-monovinyl-ω-monohydride terminated PDMS and vinyl phosphonic acid. The 10 kg mol^{-1} and 2.5 kg mol^{-1} cross-linkable brushes were named 10k* and 2.5k*, respectively, where the "*" differentiates the cross-linkable brush from the normal 1k brush. The chemical structure of the synthesized cross-linkable brushes was investigated using a combination of FTIR, GPC, ^{31}P NMR, and ^{1}H NMR, as shown in Fig. 4 (only 10k* brush characterizations are shown here, see Figure S5 for 2.5k* brush analysis). The completion of the hydrosilylation reaction was first confirmed by the disappearance of the strong silicone hydride stretching band at 2127 cm^{-1} in the FTIR spectra[53, 54], which were normalized according to the Si-CH_3 stretching band at 1256 cm^{-1}.[53, 55] GPC analysis shows a monomodal molecular weight distribution before and after the reaction, suggesting the occurrence of polymeric byproducts was successfully suppressed. The single peak around -4.5 ppm in the ^{31}P NMR spectrum can be attributed to the phosphate end group, while the ^{1}H NMR pattern exhibits the characteristic peaks attributable to the vinyl protons.[56]

The cross-linkable 10k* and 2.5k* brushes were grafted onto ZrO_2_1k nanoparticles sequentially, and each "grafting-to" step was monitored using ^{1}H NMR analysis, as shown in Fig. 5 (a) (also see Figure S6 for TGA and FTIR characterization). The incorporation of cross-linkable brushes with two different molecular weights can increase cross-linking density without deteriorating the brush-brush interpenetration. In addition, the probability of coupling between brushes of different chain lengths, i.e.10k*-10k* brush, 10k*-2.5k* brush, or 2.5k*-2.5k* brush coupling, might result in the formation of a dual network between grafted nanoparticles, which could provide an additional toughening mechanism.[49]

The processability of the ZrO_2_1k_10k*_2.5k* matrix-free nanocomposite can be tuned by changing the cross-linking agent and catalyst concentration. Using the cross-linking agent tetrakis(dimethylsiloxy)silane and Pt catalyst as an example, the nanocomposite can flow freely at room temperature without the presence of catalyst (Fig. 5 (b)), or can be cross-linked at room temperature (Fig. 5 (c), the gel point, or the crossover of the storage modulus G' and loss modulus G'', is around 25 °C). The gel point can be increased such that the nanocomposite can be molded/shaped at room temperature and then cross-linked at higher temperatures (gel point is ~95 °C in Fig. 5 (d) and (e)). The moduli can be tuned by adjusting SiH : Vinyl molar ratios. A significant decrease in storage modulus is obtained during cross-linking, probably due to secondary hydrolysis reactions of excessive SiH groups (Fig. 5 (e)).[57] A detailed discussion of the cross-linking reaction is beyond the scope of this communication. Taking advantage of the multiple degrees of control over the polymer brush system, e.g. brush graft density, brush chain length and polydispersity, and core/brush volume fraction ratio, the overall properties of the cross-linked matrix-free ZrO_2/PDMS nanocomposites can be tailored.

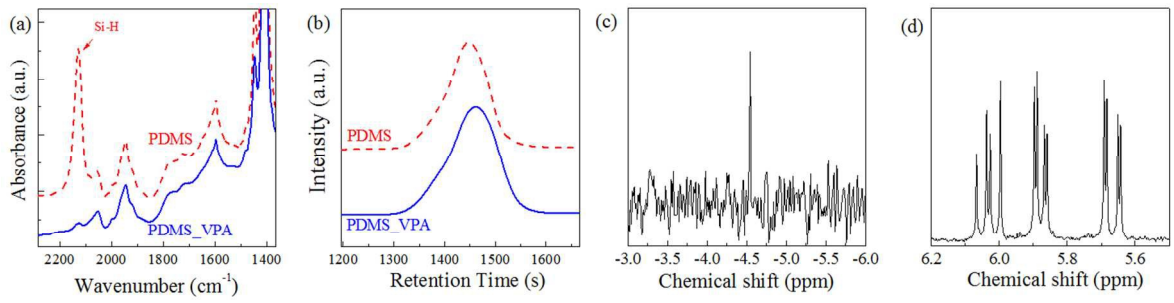

Fig. 4 (a) FTIR, (b) GPC, (c) ^{31}P NMR, and (d) ^{1}H NMR analysis of the 10k* cross-linkable brush synthesized through hydrosilylation reaction.

Cite this: DOI: 10.1039/c0xx00000x

www.rsc.org/xxxxxx

PAPER

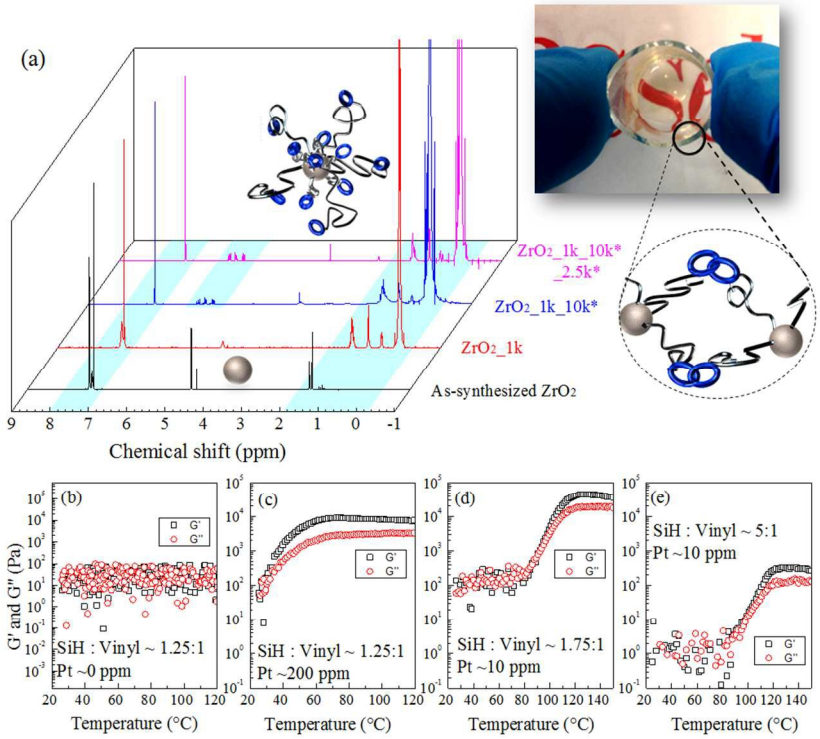

Fig. 5 (a) ^{1}H NMR spectra of as-synthesized and modified ZrO_2 nanoparticles. Cartoon shows one as-synthesized nanoparticle only stabilized by benzyl alcohol and one multimodal brush grafted cross-linkable nanoparticle. (Inset) Photograph showing a transparent matrix-free ZrO_2/PDMS nanocomposite with ~ 50 wt% ZrO_2 loading fraction. (b) to (e) The variation of the storage modulus G' and loss modulus G'' versus curing temperature for different cross-linking agent and catalyst concentration.

Experimental

LED encapsulation

To apply the transparent high-refractive-index matrix-free ZrO_2/silicone nanocomposites for well-controlled LED encapsulation, two PTFE molds with arrays of spherical-bottom wells were made. For the uncrosslinked matrix-free nanocomposites, a double-layer hemi-spherical dome configuration was created, with the matrix-free nanocomposites being the inner layer and pure silicone being the outer layer. As shown in Fig. 6 (a), the diameters of the spherical-bottom wells of the two molds are equal to the diameters of the outer and inner layer of the double–layer LED encapsulant dome, respectively. Installing detachable PTFE walls for the PTFE mold with a smaller well diameter can convert the mold into a container (Fig. 6 (b)), which can be used to make an epoxy reverse mold with arrays of hemispherical domes. The fabrication process is described in Fig. 6 (c). First, the hemi-spherical wells of the PTFE mold were filled with uncured pure silicone. The epoxy reserve mold was then fitted on top of the PTFE mold concentrically during the cross-linking of the silicone resin. The epoxy mold was released after complete cure of the silicone in step 3. In the final step, the silicone "shell" was filled with the flowable matrix-free ZrO_2/silicone nanocomposite. The dome was then mounted on a LED with the flowable matrix-free ZrO_2/silicone nanocomposite filling in the reflector cup as an adhesive. A very thin layer of pure silicone resin was finally used to "paint" the outside wall of the mounted dome to ensure structural integrity. Since the high RI nanocomposite in the inner layer is directly in contact with the LED die, the double-layer encapsulant dome can increase the light extraction at the die / nanocomposite interface. Given the spherical geometry of the double-layer dome, the total internal reflection at the nanocomposite / silicone interface and the silicone / air interface is significantly alleviated.

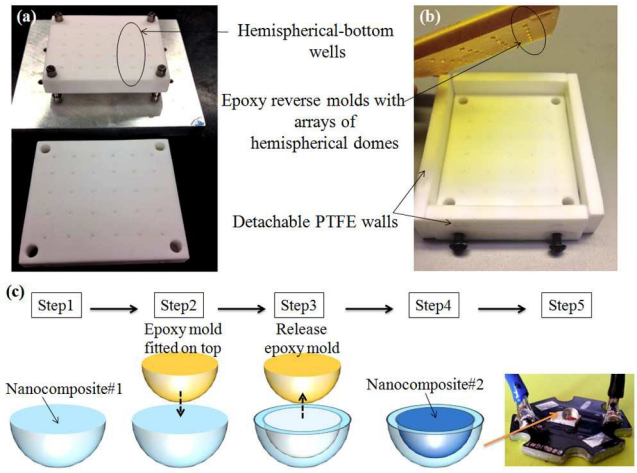

Fig. 6 Photographs of (a) PTFE molds and (b) epoxy reverse mold. Illustration of the fabrication process of a double-layer hemispherical LED encapsulate dome (Inset photograph of a LED mounted with the dome).

Synthesis of cross-linkable PDMS brushes

As shown in Scheme 3. The cross-linkable PDMS brushes were synthesized through a hydrosilylation reaction between α-monovinyl-ω-monohydride terminated PDMS (Gelest, DMS-HV15 with Mw = 2,500 g/mol and DMS-HV22 with Mw = 10,000 g/mol) and vinyl phosphonic acid (Sigma-Aldrich, VPA), which involves the addition of a silicon hydride (Si-H) bond across a carbon-carbon double bond in the presence of platinum complexes.[58, 59] In a typical reaction, 0.6 mmol of DMS-HV15 or DMS-HV22 was dissolved in 180 mL THF. Subsequently, 20 mL THF solution of platinum(0)-1,3-divinyl-1,1,3,3-tetramethyldisiloxane complex (Sigma-Aldrich) was added slowly under stirring, where the Pt concentration was designated to be 40 ppm.[60] 1.8 mmol of VPA was then added dropwise, and the mixture was refluxed at 70 °C for 24 hours. The modified PDMS in THF was precipitated using methanol and put in the centrifuge at 11,000 rpm for 10 min. The supernatant containing unreacted VPA and other byproducts was removed. The purified transparent cross-linkable PDMS brush polymers were put in a vacuum oven for 2 hours to remove any residual solvents.

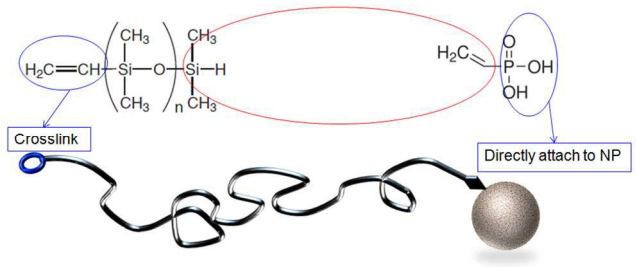

Scheme 3 Illustration of the synthesis of a cross-linkable PDMS brush.

Conclusions

"Matrix-free" nanocomposites with a bimodal population of polymer brushes are an excellent strategy to optimize filler loading while maintaining random dispersion. The surface bound polymer brushes not only provide structural integrity, but also stabilize filler dispersion. A multimodal brush configuration is important to ensure sufficient monomer crowding near the nanoparticle surface to screen the core-core attraction, meanwhile facilitating long brush entanglement and interpenetration at low brush volumes. Therefore, the most promising "matrix-free" nanocomposite should have at least one short brush population effectively filling nanofiller interstitial space and preventing micro-phase separation, and one long brush population with a molecular weight comparable to M_e to ensure at least one "entanglement" per chain to suppress crack propagation. The current study demonstrates the use of "matrix-free" nanocomposites by incorporating more than 50 wt% ZrO_2 nanoparticle loading in PDMS without sacrificing optical transparency, leading to promising applications in high-refractive-index high-efficiency LED encapsulants.

Acknowledgment

This work was supported primarily by the Engineering Research Centers Program (ERC) of the National Science Foundation under NSF Cooperative Agreement No. EEC-0812056 and in part by New York State under NYSTAR contract C090145. The authors also acknowledge the financial support from the Nanoscale Science and Engineering Initiative of the National Science Foundation under NSF award number DMR-0642576. The authors gratefully thank Matthew Ravalli and Anthony Maiorana for help with rheological measurements, Charles S.S. Goodwin for help with aging tests, Jianing Gao for PTFE mold design, and Prolight Opto Technology Corporation for providing un-capped LEDs. We also thank Professor Robert F. Karlicek for inspiring discussions.

Notes and references

[a] *Department of Materials Science and Engineering, Rensselaer Polytechnic Institute, Troy, New York 12180, USA. E-mail: liy20.rpi@gmail.com*
[b] *Department of Chemistry and Biochemistry, University of South Carolina, Columbia, South Carolina 29208, USA.*
[c] *State Key Laboratory of Metal Matrix Composites, School of Materials Science and Engineering, Shanghai Jiao Tong University, Shanghai 200240, PR China.*

† Electronic Supplementary Information (ESI) available: [experimental details and instrumentations]. See DOI: 10.1039/b000000x/

1. S. Kango, S. Kalia, A. Celli, J. Njuguna, Y. Habibi and R. Kumar, *Prog. Polym. Sci.*, 2013, **38**, 1232–1261.
2. S. K. Kumar and R. Krishnamoorti, *Annu. Rev. Chem. Biomol. Eng.*, 2010, **1**, 37-58.
3. J. Jancar, J. F. Douglas, F. W. Starr, S. K. Kumar, P. Cassagnau, A. J. Lesser, S. S. Sternstein and M. J. Buehler, *Polymer*, 2010, **51**, 3321-3343.
4. B. M. Novak, *Adv. Mater.*, 1993, **5**, 422-433.
5. F. W. Mont, J. K. Kim, M. F. Schubert, E. F. Schubert and R. W. Siegel, *J. Appl. Phys.*, 2008, **103**, 1-6.
6. A. B. Bourlinos, S. Ray Chowdhury, R. Herrera, D. D. Jiang, Q. Zhang, L. A. Archer and E. P. Giannelis, *Adv. Funct. Mater.*, 2005, **15**, 1285-1290.

7. A. B. Bourlinos, R. Herrera, N. Chalkias, D. D. Jiang, Q. Zhang, L. A. Archer and E. P. Giannelis, *Adv. Mater.*, 2005, **17**, 234-237.
8. D. Kim, Y. Kim and J. Cho, *Chem. Mater.*, 2013, **25**, 3834-3843.
9. Y. Zheng, J. Zhang, L. Lan, P. Yu, R. Rodriguez, R. Herrera, D. Wang and E. P. Giannelis, *ChemPhysChem*, 2010, **11**, 61-64.
10. S. Srivastava, J. L. Schaefer, Z. Yang, Z. Tu and L. A. Archer, *Adv. Mater.*, 2014, **26**, 201-234.
11. M. N. Tchoul, S. P. Fillery, H. Koerner, L. F. Drummy, F. T. Oyerokun, P. A. Mirau, M. F. Durstock and R. A. Vaia, *Chem. Mater.*, 2010, **22**, 1749-1759.
12. I. Yilgor, T. Eynur, E. Yilgor and G. L. Wilkes, *Polymer*, 2009, **50**, 4432-4437.
13. J. Choi, C. M. Hui, J. Pietrasik, H. Dong, K. Matyjaszewski and M. R. Bockstaller, *Soft Matter*, 2012, **8**, 4072-4082.
14. B. I. Dach, H. R. Rengifo, N. J. Turro and J. T. Koberstein, *Macromolecules*, 2010, **43**, 6549-6552.
15. Y. Li, P. Tao, A. Viswanath, B. C. Benicewicz and L. S. Schadler, *Langmuir*, 2012, **29**, 1211-1220.
16. P. Tao, A. Viswanath, Y. Li, R. W. Siegel, B. C. Benicewicz and L. S. Schadler, *Polymer*, 2013, **54**, 1639–1646.
17. B. Natarajan, T. Neely, A. Rungta, B. C. Benicewicz and L. S. Schadler, *Macromolecules*, 2013, **46**, 4909–4918.
18. H.-Y. Yu and D. L. Koch, *Langmuir*, 2010, **26**, 16801-16811.
19. N. Dan and M. Tirrell, *Macromolecules*, 1993, **26**, 6467-6473.
20. S. R. Edgecombe, J. M. Gardiner and M. W. Matsen, *Macromolecules*, 2002, **35**, 6475-6477.
21. M. Wong, J. Guenther, L. Sun, J. Blümel, R. Nishimura and H. J. Sue, *Adv. Funct. Mater.*, 2012, **22**, 3614-3624.
22. R. Francis, N. Joy, E. Aparna and R. Vijayan, *Polymer Reviews*, 2014, **54**, 268-347.
23. P. Tao, Y. Li, R. W. Siegel and L. S. Schadler, *J. Mater. Chem. C*, 2013, **1**, 86-94.
24. Y. Li, T. M. Krentz, L. Wang, B. C. Benicewicz and L. S. Schadler, *ACS Appl. Mater. Interfaces*, 2014, **6**, 6005-6021.
25. T. B. Martin and A. Jayaraman, *Macromolecules*, 2013, **46**, 9144-9150.
26. G. Garnweitner, L. M. Goldenberg, O. V. Sakhno, M. Antonietti, M. Niederberger and J. Stumpe, *Small*, 2007, **3**, 1626-1632.
27. C. Lü and B. Yang, *J. Mater. Chem.*, 2009, **19**, 2884-2901.
28. U. Anselmi-Tamburini, J. N. Woolman and Z. A. Munir, *Adv. Funct. Mater.*, 2007, **17**, 3267-3273.
29. M. A. White, J. A. Johnson, J. T. Koberstein and N. J. Turro, *J. Am. Chem. Soc.*, 2006, **128**, 11356-11357.
30. B. Zhang, T. Kong, W. Xu, R. Su, Y. Gao and G. Cheng, *Langmuir*, 2010, **26**, 4514-4522.
31. M. Kobayashi, R. Matsuno, H. Otsuka and A. Takahara, *Sci. Tech. Adv. Mater.*, 2006, **7**, 617-628.
32. D. Dukes, Y. Li, S. Lewis, B. Benicewicz, L. Schadler and S. K. Kumar, *Macromolecules*, 2010, **43**, 1564-1570.
33. T. Wu, K. Efimenko, P. Vlcˇek, V. Šubr and J. Genzer, *Macromolecules*, 2003, **36**, 2448-2453.
34. Y. Wu, X. Zhao, F. Li and Z. Fan, *J. Electroceram.*, 2003, **11**, 227-239.
35. T. Kyprianidou-Leodidou, W. Caseri and U. W. Suter, *J. Phys. Chem.*, 1994, **98**, 8992-8997.
36. Y. Rao and S. Chen, *Macromolecules*, 2008, **41**, 4838-4844.
37. M. M. Demir, K. Koynov, Ü. Akbey, C. Bubeck, I. Park, I. Lieberwirth and G. Wegner, *Macromolecules*, 2007, **40**, 1089-1100.
38. W. Caseri, *Macromol. Rapid Commun.*, 2000, **21**, 705-722.
39. W. Caseri, *Chem. Eng. Commun.*, 2008, **196**, 549-572.
40. L. Filion and M. Dijkstra, *Phys. Rev. E*, 2009, **79**, 046714.
41. H. Koerner, L. F. Drummy, B. Benicewicz, Y. Li and R. A. Vaia, *ACS Macro Lett.*, 2013, **2**, 670-676.
42. H.-Y. Yu and D. L. Koch, *Langmuir*, 2013, **29**, 8197-8202.
43. J. Choi, C. M. Hui, M. Schmitt, J. Pietrasik, S. Margel, K. Matyjazsewski and M. R. Bockstaller, *Langmuir*, 2013, **29**, 6452-6459.
44. Y. Cheng, C. Lu and B. Yang, *Recent Pat. Mat. Sci.*, 2011, **4**, 15-27.
45. L. Fetters, D. Lohse and R. Colby, in *Physical properties of polymers handbook*, Springer, 2007, pp. 447-454.
46. P. Longin, C. Verdier and M. Piau, *J. Non-newton. Fliud*, 1998, **76**, 213-232.
47. Y. H. Zang and P. J. Carreau, *J. Appl. Polym. Sci.*, 1991, **42**, 1965-1968.
48. T. C. McLeish and S. T. Milner, in *Branched Polymers II*, Springer, 1999, pp. 195-256.
49. R. A. Mrozek, P. J. Cole, K. J. Otim, K. R. Shull and J. L. Lenhart, *Polymer*, 2011, **52**, 3422-3430.
50. C. Creton, E. J. Kramer and G. Hadziioannou, *Macromolecules*, 1991, **24**, 1846-1853.
51. C.-A. Dai, E. J. Kramer, J. Washiyama and C.-Y. Hui, *Macromolecules*, 1996, **29**, 7536-7543.
52. M. Ma, F. W. Mont, X. Yan, J. Cho, E. F. Schubert, G. B. Kim and C. Sone, *Opt. Express*, 2011, **19**, A1135-A1140.
53. D. W. Chung and T. G. Kim, *J. Ind. Eng. Chem.*, 2007, **13**, 979-984.
54. D. A. Brown and G. J. Price, *Polymer*, 2001, **42**, 4767-4771.
55. L. Sacarescu, R. Ardeleanu, G. Sacarescu and M. Simionescu, *Eur. Polym. J.*, 2004, **40**, 57-62.
56. J. R. Parikh and W. E. Doering, *J. Am. Chem. Soc.*, 1967, **89**, 5505-5507.
57. T. Simpson, Z. Tabatabaian, C. Jeynes, B. Parbhoo and J. Keddie, *J. Polym. Sci., Part A: Polym. Chem.*, 2004, **42**, 1421-1431.
58. W. Caseri and P. S. Pregosin, *Organometallics*, 1988, **7**, 1373-1380.
59. L. N. Lewis, J. Stein, Y. Gao, R. E. Colborn and G. Hutchins, *Platinum Met. Rev.*, 1997, **41**, 66-74.
60. D. W. Chung and T. G. Kim, *J. Ind. Eng. Chem.*, 2007, **13**, 571-577.

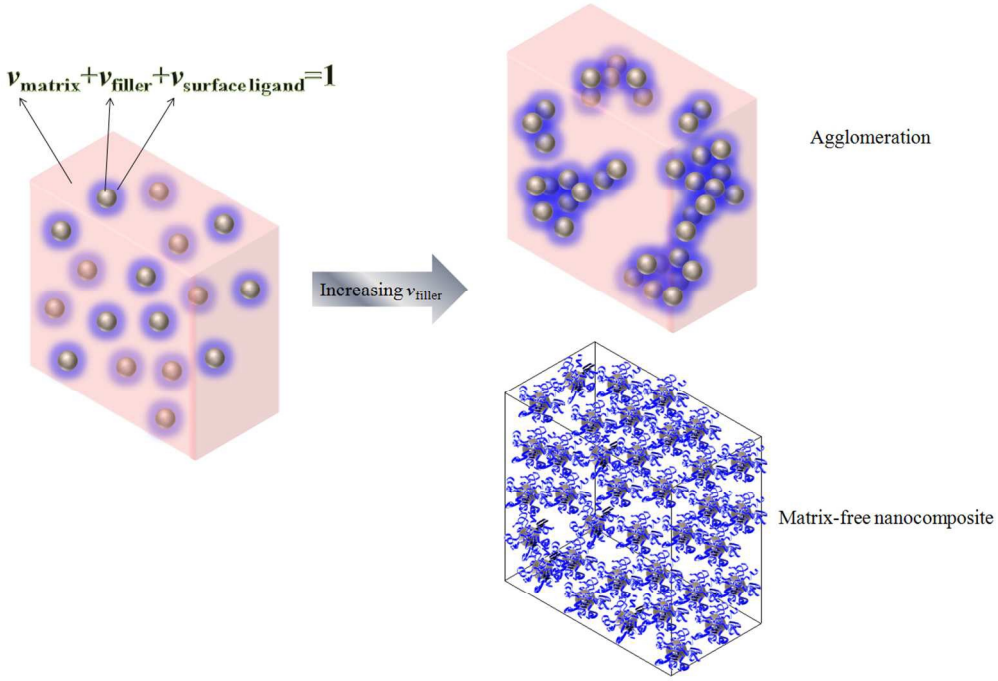

(Left) Illustration of a conventional three-component polymer nanocomposite system and (right) comparison of nanoparticle agglomeration versus matrix-free nanocomposite for maximized nanocomposite performance enhancement.
347x244mm (96 x 96 DPI)

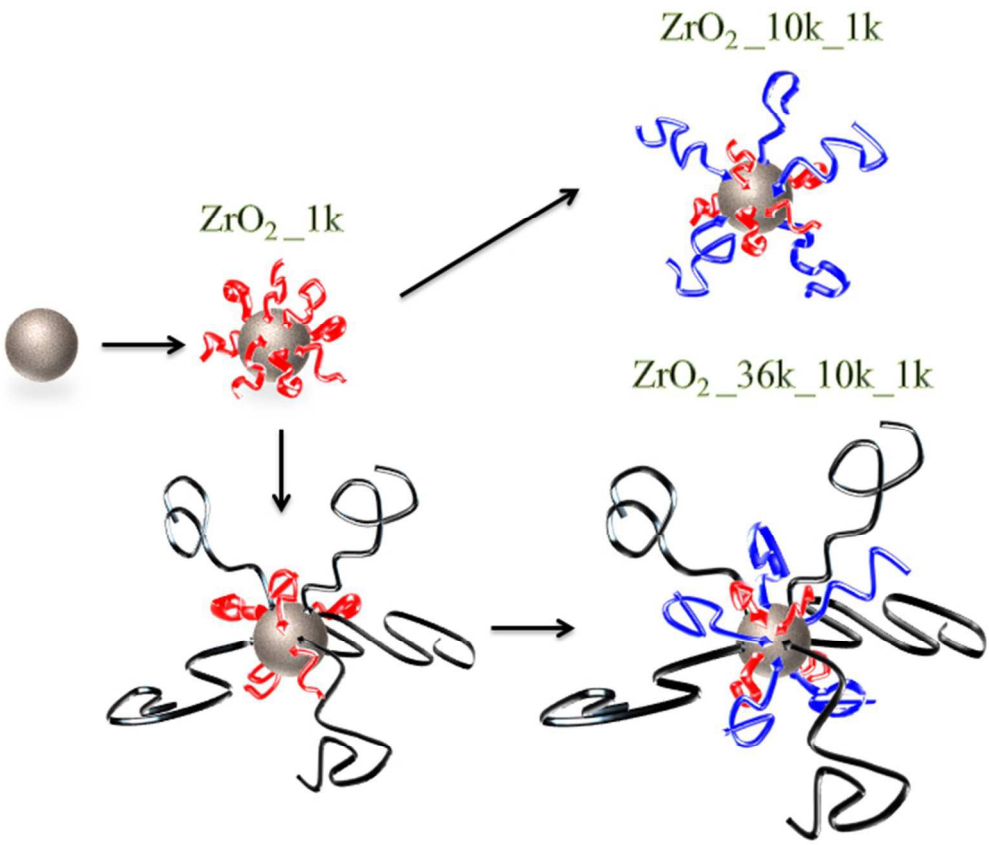

Schematic illustration of the preparation of ZrO2_1k, ZrO2_1k_10k, and ZrO2_1k_36k_10k nanoparticles via a multiple-step "grafting-to" process
188x159mm (96 x 96 DPI)

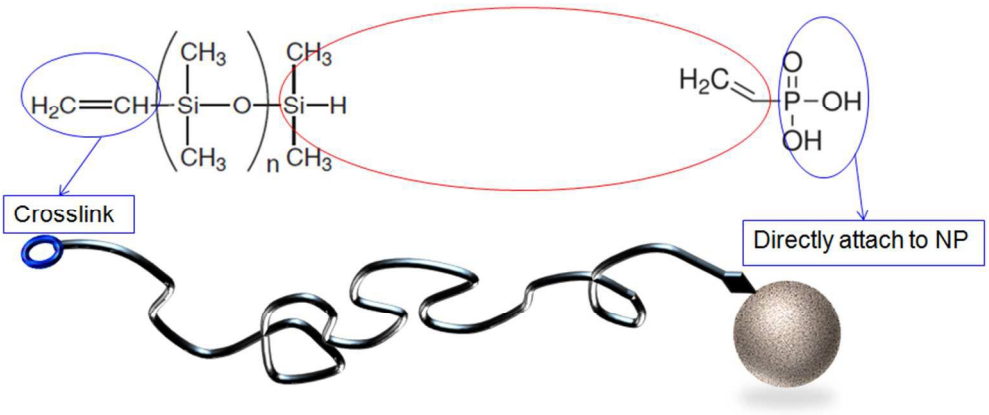

Illustration of the synthesis of a cross-linkable PDMS brush
253x105mm (96 x 96 DPI)

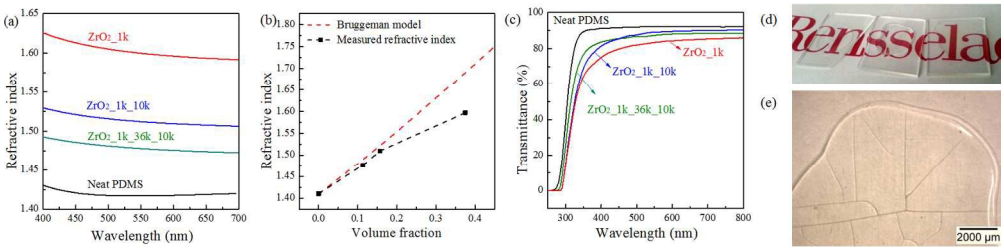

Fig. 1 (a) Refractive index dispersion of neat PDMS and "matrix-free" ZrO2/PDMS nanocomposites with three different v_"filler" . (b) Comparison of measured refractive indices at 633 nm with the Bruggeman model. (c) UV-Vis spectra of the three types of "matrix-free" nanocomposites. (d) Photograph shows the appearance of the ~0.5 mm thick samples. (e) Photograph showing crack propagation in the ZrO2_1k sample after one month.
486x118mm (96 x 96 DPI)

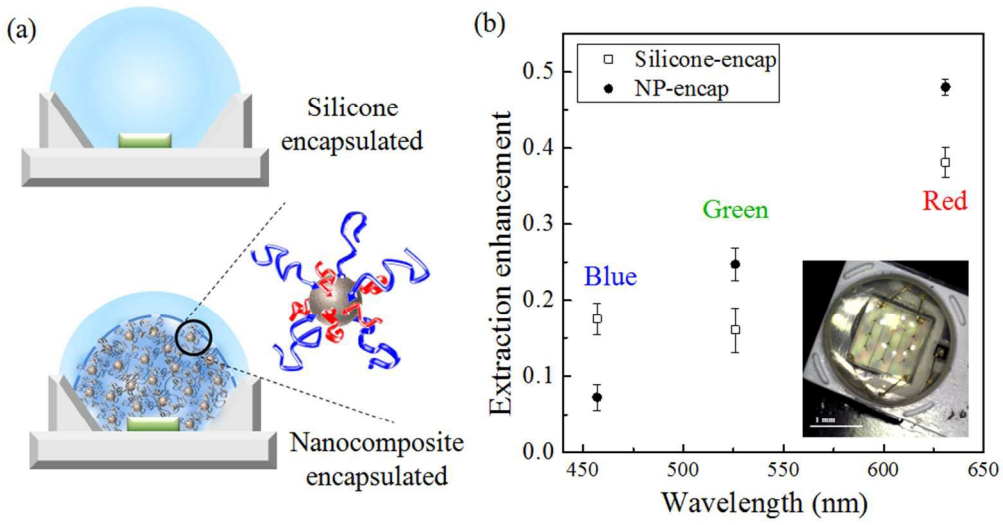

(a) Illustrative cross-section of commercial silicone encapsulated LED and nanocomposite encapsulated LED. (b) Light extraction enhancement after encapsulation of commercial silicone and the ZrO2_10k_1k nanocomposite/silicone double-layer. Inset photograph of a nanocomposite encapsulated green LED.
266x138mm (96 x 96 DPI)

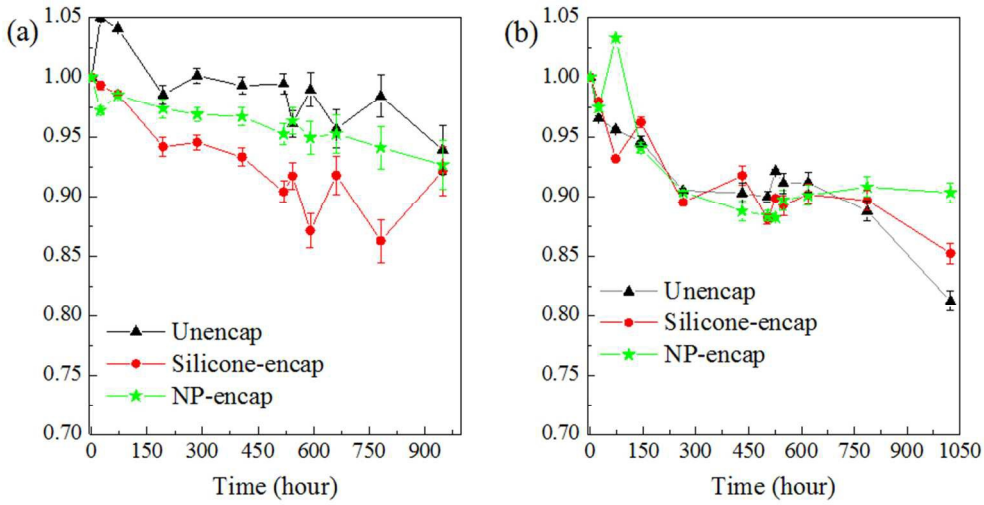

The degradation of optical output power for different green LED packages. LED forward current was maintained at (a) 100±3% mA for 500 hours and then 350±3% mA for 500 hours; (b) 500±3% mA for 500 hours and then 1000±3% mA for 500 hours.
248x125mm (96 x 96 DPI)

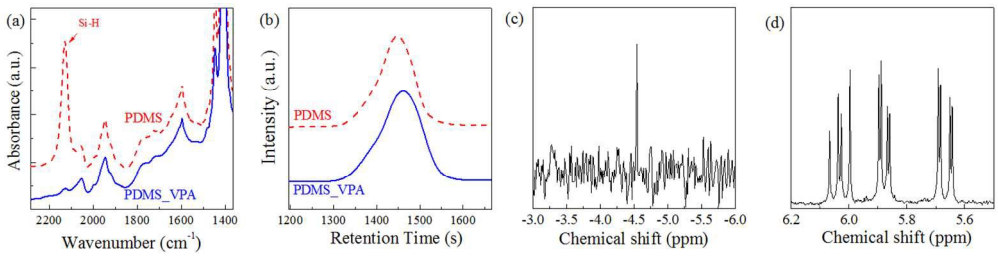

(a) FTIR, (b) GPC, (c) 31P NMR, and (d) 1H NMR analysis of the 10k* cross-linkable brush synthesized through hydrosilylation reaction.
385x100mm (96 x 96 DPI)

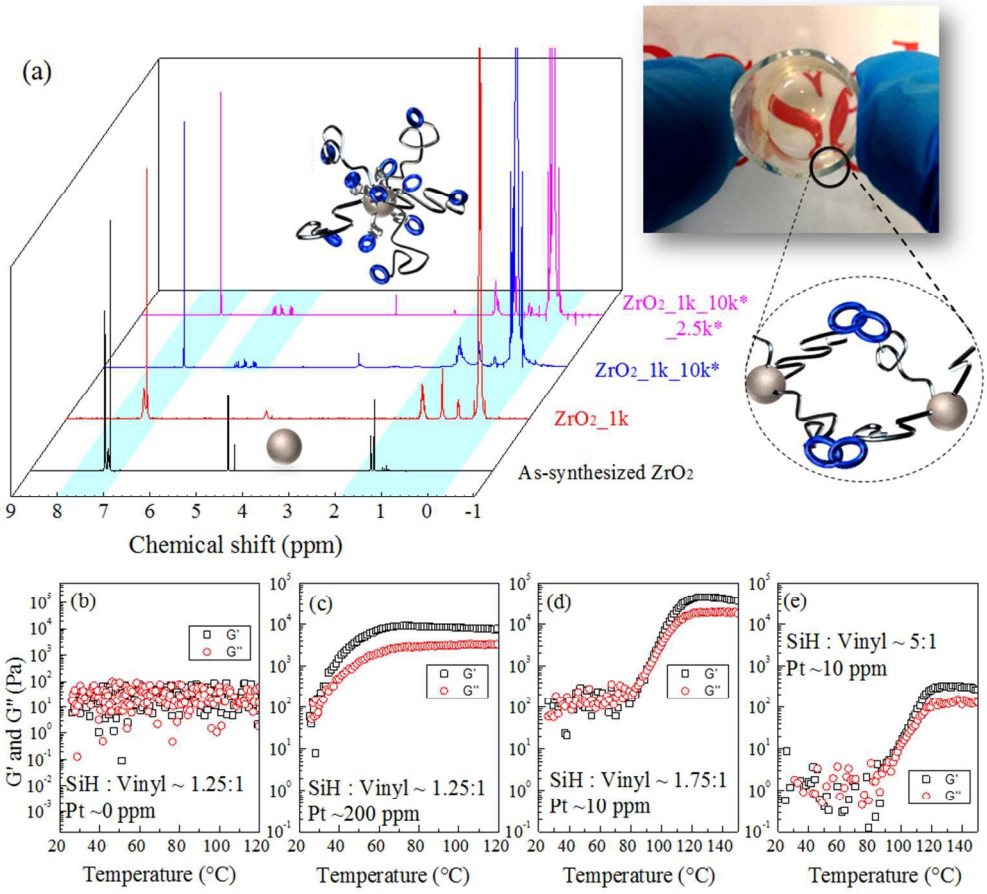

(a) 1H NMR spectra of as-synthesized and modified ZrO2 nanoparticles. Cartoon shows one as-synthesized nanoparticle only stabilized by benzyl alcohol and one multimodal brush grafted cross-linkable nanoparticle. (Inset) Photograph showing a transparent matrix-free ZrO2/PDMS nanocomposite with ~ 50 wt% ZrO2 loading fraction. (b) to (e) The variation of the storage modulus G′ and loss modulus G′′ versus curing temperature for different cross-linking agent and catalyst concentration.
268x243mm (96 x 96 DPI)

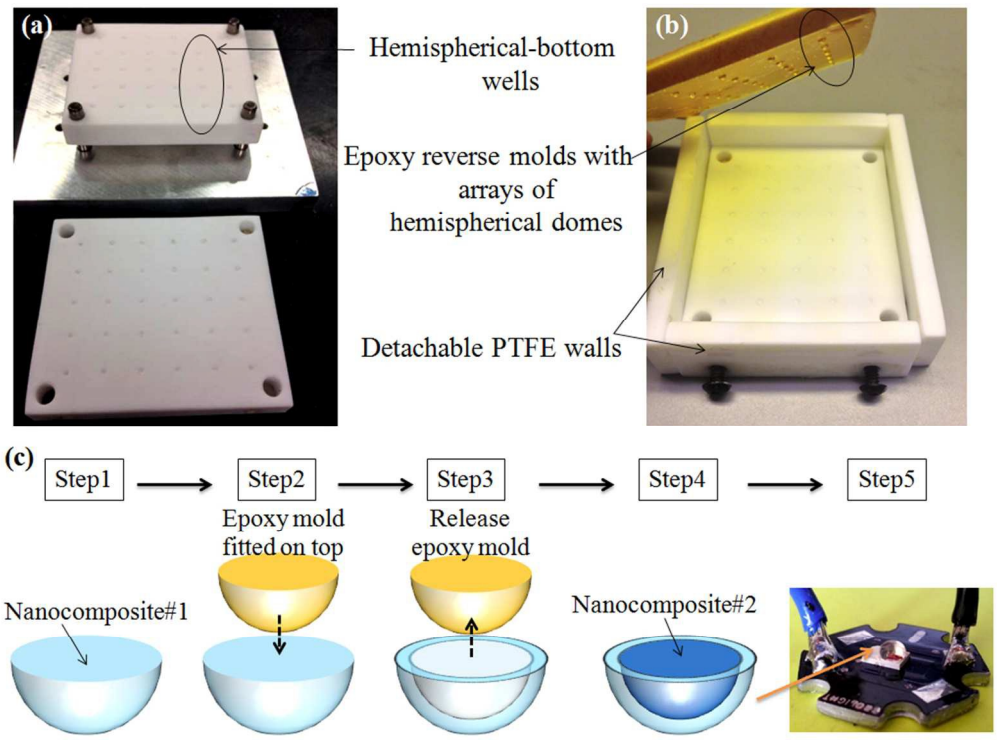

Photographs of (a) PTFE molds and (b) epoxy reverse mold. Illustration of the fabrication process of a double-layer hemispherical LED encapsulate dome (Inset photograph of a LED mounted with the dome).
270x199mm (96 x 96 DPI)